Effects of Tightening Torque on Dynamic Characteristics of Low Pressure Rotors Connected by a Spline Coupling

Chen Xi, *Liao Mingfu* *, *Li Quankun*

Institute of Monitoring and Control for Rotating Machinery and Wind Turbines, School of Power and Energy, Northwestern Polytechnical University, Xi′an 710129, P. R. China

(Received 9 June 2015; revised 22 February 2016; accepted 26 July 2016)

Abstract: A rotor dynamic model is built up for investigating the effects of tightening torque on dynamic characteristics of low pressure rotors connected by a spline coupling. The experimental rotor system is established using a fluted disk and a speed sensor which is applied in an actual aero engine for speed measurement. Through simulating calculation and experiments, the effects of tightening torque on the dynamic characteristics of the rotor system connected by a spline coupling including critical speeds, vibration modes and unbalance responses are analyzed. The results show that when increasing the tightening torque, the first two critical speeds and the amplitudes of unbalance response gradually increase in varying degrees while the vibration modes are essentially unchanged. In addition, changing axial and circumferential positions of the mass unbalance can lead to various amplitudes of unbalance response and even the rates of change.

Key words: tightening torque; dynamic characteristics; spline coupling; low pressure rotor; aero engine

CLC number: V231.96 **Document code**: A **Article ID**: 1005-1120(2017)05-0514-10

0 Introduction

Spline couplings are widely used in high-speed rotating machinery, especially modern aero engines. In order to improve thrust-weight ratio of high bypass ratio turbofan engines, an inter-bearing is normally used to support one end of the high-pressure rotor and to connect the high-pressure rotor with the low-pressure rotor in a dual rotor system. This structure can make a strong coupling to the engine structure. For reducing vibration and deformation of the low-pressure rotor and the effect of low-pressure rotor on high-pressure rotor, a turbine shaft and a fan shaft are often connected by a spline coupling.

Many researchers have conducted extensive investigation about the influence of spline couplings on dynamic characteristics of rotor systems. Marmol et al.[1] derived four linearized mechanical parameters characterizing a side fit spline coupling including radial stiffness, radial damping coefficients, angular stiffness and angular damping coefficients. Ku et al.[2] quantified the angular stiffness and equivalent viscous damping coefficients of an axial spline coupling and found that the damping contributes to the cross-coupling in terms of the angular stiffness matrix. Tjernberg[3] presented a finite element model and an analytical model for the load distribution in the axial direction of a spline coupling and the torque transfer between the shaft and the sleeve. The result showed that the best way to uniform the load distribution is to vary the thickness of the spline tooth in the axial direction. Al-Hussain[4] studied the effect of angular misalignment on the stability of two rotors coupled through a flexible mechanical coupling. An increase in angular misalignment or mechanical coupling stiffness leads to an increase of the model stability region. Li et al.[5] established a calculation model for a spline joint

* Corresponding author, E-mail address: mfliao@nwpu.edu.cn.

How to cite this article: Chen Xi, Liao Mingfu, Li Quankun. Effects of tightening torque on dynamic characteristics of low pressure rotors connected by a spline coupling[J]. Trans. Nanjing Univ. Aero. Astro., 2017,34(5):514-523.
http://dx.doi.org/10.16356/j.1005-1120.2017.05.514

structure using the contact finite element method and performed dynamic analysis on the spline coupling. Although a variety of research results involve the effect of spline couplings on dynamic characteristics of rotors, the majority were basically aimed at the specific structure of spline coupling, i. e., two shafts with external teeth are matched with a sleeve with internal teeth. In contrast, the research on the structure of rigid spline couplings, i. e., an axial nut connecting a shaft with external teeth and another shaft with internal teeth, was still limited to theoretical analysis or simulating calculation, but few experiments.

In view of this situation, this paper will take the rigid spline coupling connecting a turbine shaft with a fan shaft in the low-pressure rotor of aero engine as the research object. Referring to the typical structure of spline couplings in the low-pressure rotors of high bypass ratio turbofan engines, the rotor modeling is established, finite element calculation on dynamic characteristics of rotor model is performed, and a rotor dynamics testing system with a fluted disk and a speed sensor is established. Experiments about the effects of tightening torque of the axial nut on the dynamic characteristics are conducted, which can provide a reference for the design and application on this type of spline coupling.

1 Rotor Modeling

The structure of the spline coupling in the low-pressure rotor of the CFM-56 engine, adopts a combination of a spline for torque transmitting, cylindrical surface at both ends for centering and an axial nut for tightening, as shown in Fig. 1[6]. As a consequence, the tightening torque of the axial nut directly affects the connection status of the spline coupling.

The structure is the primary consideration in the design process of the rotor dynamic model. The suitability and completeness of the structure are the foundation of components design and the necessary conditions of best approximation to the real aircraft engines in order to adequately reflect the dynamic behaviors.

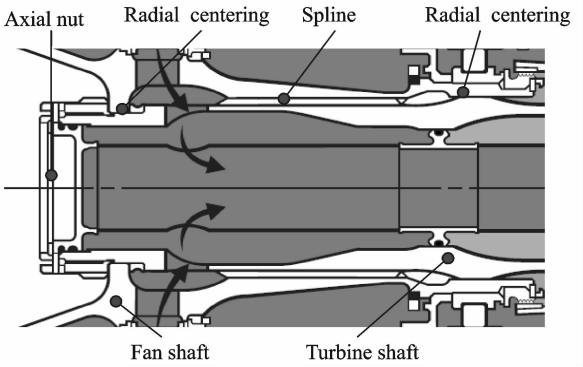

Fig. 1 Structure of CFM-56 spline coupling

To study the dynamic characteristics of low-pressure rotors with spline coupling, the experimental rotor system should be designed to meet the following criteria:

(1) The structure should be convenient for installation, commissioning and disassembly.

(2) The rotating speed should be higher than the second-order critical speed, and continuously variable speed should be realized in the control process.

(3) The experimental rotor system should have similar dynamic characteristics with the low-pressure rotor in real aero engine CFM-56.

(4) Experiments on dynamic characteristics of the rotor system can be conducted and corresponding vibration parameters can be measured accurately.

(5) The effect of tightening torque on the dynamic characteristics of rotor system can be further studied and discussed by means of experiments.

According to engineering practice, the first-order critical speed of the low-pressure rotor in CFM-56 is about 2 400 r/min and the second-order critical speed is about 3 600 r/min[6]. Using the design principle of similarity[7] in mechanical systems to ensure the similarity of structure and dynamic characteristics, and considering the actual operating condition and the parameters such as the motor′s rated power, the first-order critical speed of the experimental rotor system is eventually designed to reach 2 000—2 500 r/min and the second-order critical speed is ultimately designed

to reach 3 000—3 500 r/min.

Referring to the actual structure of the low-pressure rotors in CFM-56 aero engine and the experimental design principles, the overall structure of the rotor dynamic model is determined, as shown in Fig. 2.

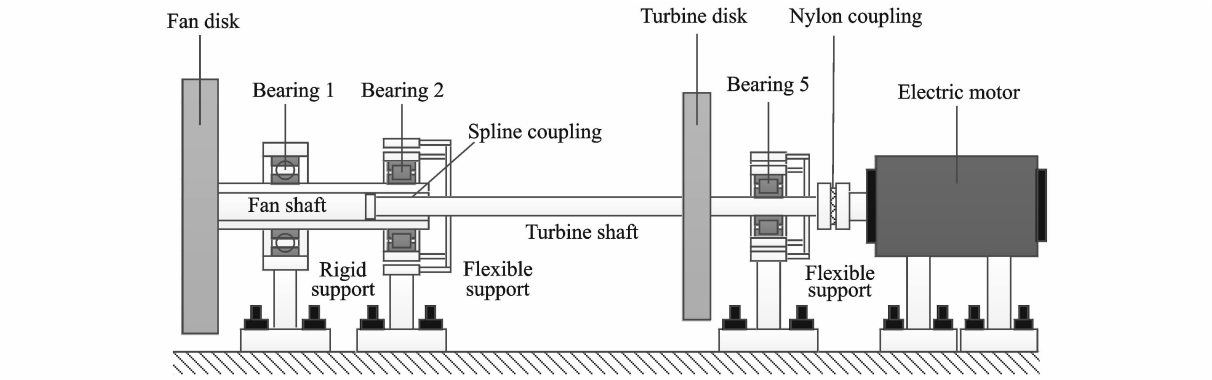

Fig. 2 Schematic diagram of rotor dynamics test rig

In order to reduce the sensitivity of unbalance response and avoid instability caused by self-excited vibration, the first-order and second-order bending strain energy of the rotor-bearing system should be calculated using the finite element simulation software ANSYS[8].

According to the design criteria for rotor-bearing system, the bending strain energy of the rotor components should not exceed 25%[9] of the total strain energy of system when the operating speed is equal or close to the critical speed. As listed in Table 1, the first-order and second-order bending strain energy of the rotor system are respectively 16.256% and 20.372% of the total strain energy, which both meet the design requirement.

Table 1 Bending strain energy of rotor system

Critical speed	Bending strain energy/%
First-order	16.256
Second-order	20.372

The supporting mode of three bearings is 0—2—1, i.e., no bearings in front of the fan, two bearings between the fan and the turbine, and one bearing in rear of the turbine. The fan and the low-pressure compressors are simplified as the fan disk, which is mounted on the fan shaft through the cylindrical surface centering and bolted flange connecting; while the turbine is simplified as the turbine disk, which is mounted on the turbine shaft through conical surface matching and round nut tightening. Using the spline coupling and the axial nut, the fan shaft can be rigidly connected with the turbine shaft.

2 Dynamics Calculation

The two-dimensional finite element model of the rotor system is presented in Fig. 3. Both the fan shaft and the turbine shaft adopt the Timoshenko beam element (Beam 188) considering bending and shear deformation. In addition to the fan disk, the turbine disk also adopts the concentrated mass element (Mass 21). Three supports adopt the spring element (Combin 14) considering tension and compression stiffness. The spline coupling is simplified as a special shaft segment with a certain lateral and angular stiffness, combining the element (Beam 188) with the element (Combin 14).

In order to achieve the design requirements of the first two critical speeds, through optimizing calculation, the stiffness of three supports can be selected. According to the previous experimental rotors in lab, the range of supports stiffness K_1, K_2 and K_5 are supposed to be (1—9)$\times 10^8$, (1—5)$\times 10^6$ and (1—5)$\times 10^6$ N·m^{-1}, respectively. The first two critical speeds of the system with different supporting stiffness combi-

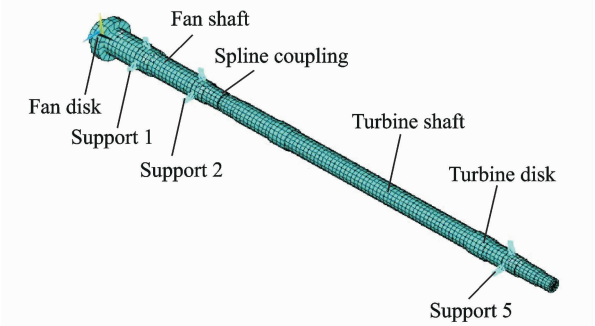

Fig. 3 Finite element model of rotor system

nations are calculated and the effects of supporting stiffness on critical speeds are discussed.

As shown in Figs. 4, 5, when K_1 keeps constant, the first-order and second-order critical speeds both increase with the increment of K_2 and K_5. As shown in Fig. 6, with different supporting stiffness combinations, the general trend is that the first-order critical speed goes up at first and then level off with the increase of K_1, while the second-order critical speed goes up continuously.

In summary, in order to achieve the design requirements of the first two critical speeds, K_1, K_2 and K_5 are selected to reach 1×10^8, $(1—2)\times10^6$ and $(1—2)\times10^6$ N·m^{-1}, respectively. On

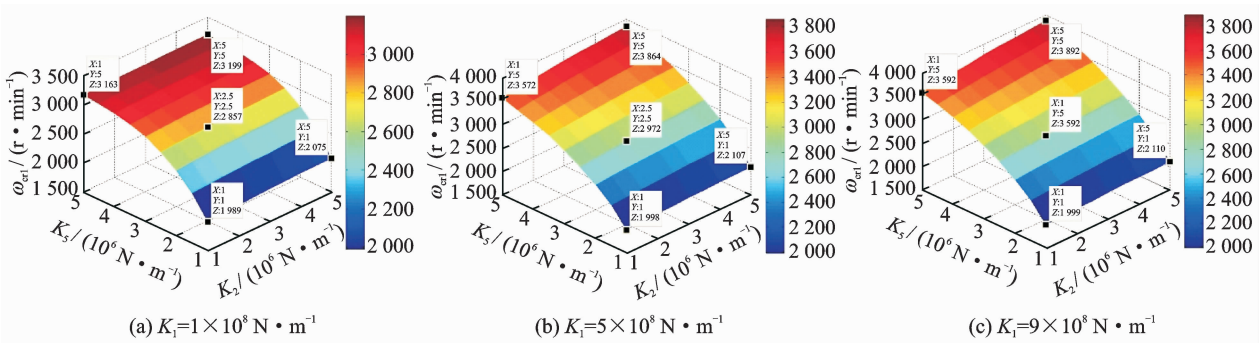

(a) $K_1=1\times10^8$ N·m^{-1} (b) $K_1=5\times10^8$ N·m^{-1} (c) $K_1=9\times10^8$ N·m^{-1}

Fig. 4 Three-dimensional plot on the first-order critical speed

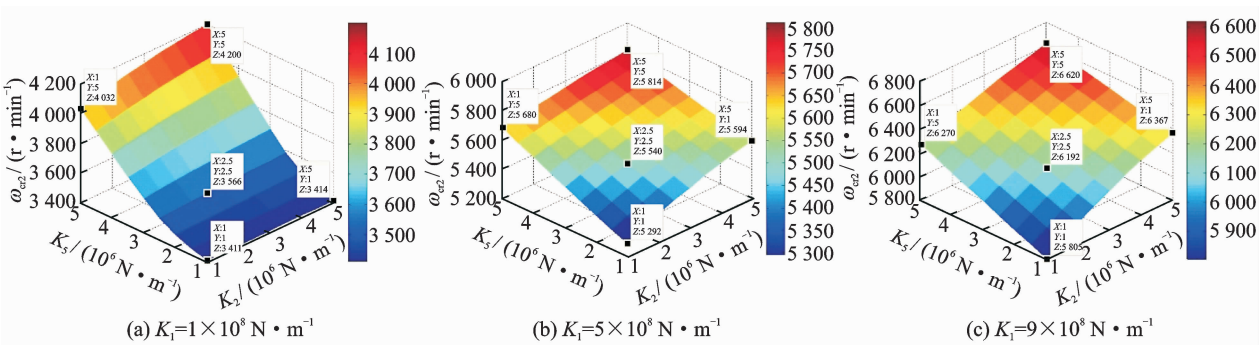

(a) $K_1=1\times10^8$ N·m^{-1} (b) $K_1=5\times10^8$ N·m^{-1} (c) $K_1=9\times10^8$ N·m^{-1}

Fig. 5 Three-dimensional plot on the second-order critical speed

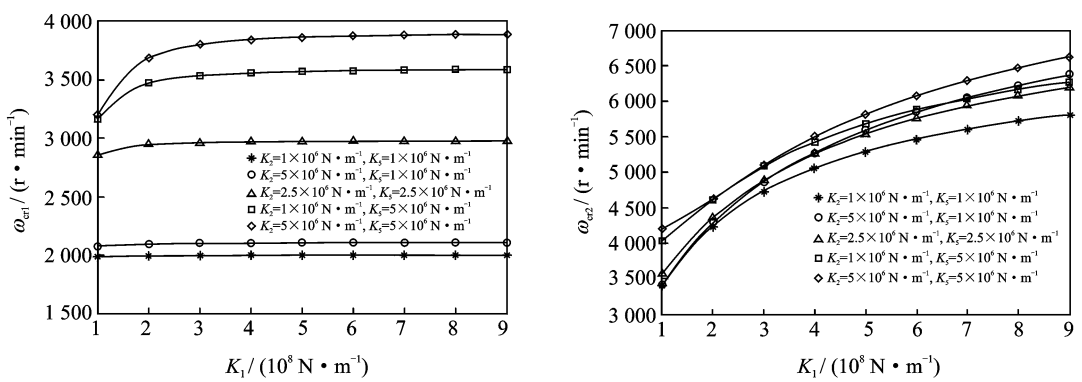

(a) The first-order critical speed (b) The second-order critical speed

Fig. 6 Critical speeds varying with supporting stiffness combinations

this basis, the stiffness of three supports are calculated using ANSYS three-dimensional model and the specific values K_1, K_2 and K_5 are 1×10^8, 1.3×10^6 and 1.4×10^6 N·m^{-1}, respectively, which are in the range of optimizing calculation.

Under the condition of the selected supporting stiffness, the Campbell diagram of critical speeds using finite element method is presented in Fig. 7. The first critical speed ω_{cr1} is equal to 2 298.515 r/min and the second critical speed ω_{cr2} is equal to 3 345.339 r/min, which basically meets the design requirements. And the vibration modes corresponding to the first two critical speeds are shown in Fig. 8.

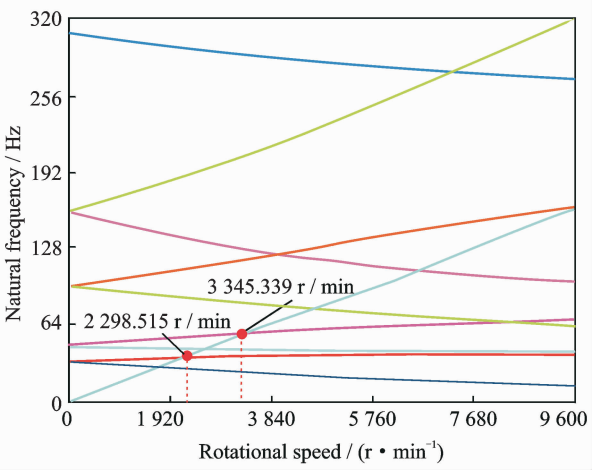

Fig. 7 Campbell diagram of critical speeds

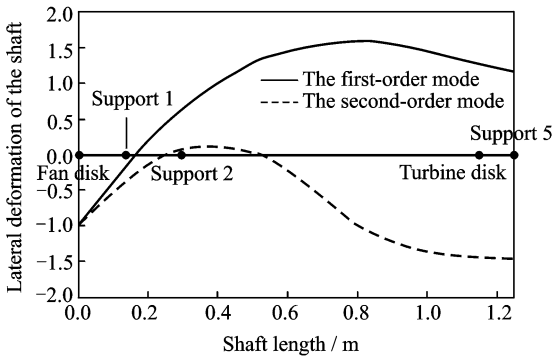

Fig. 8 The first two vibration modes

3 Experimental Analysis

3.1 Experimental rotor system

In order to measure vibration signals, the displacement sensors are installed in the horizontal and vertical direction, as shown in Fig. 9. As shown in Fig. 10, the rotational speed signal is measured by a fluted disk and a speed sensor (GZ-67 speed sensor) which is applied in actual aero engines. The speed signal processing is shown in Fig. 11. In this way, accurate speed signals and stable phases can be obtained.

The strength of rotating components such as coupling and shafts are checked, and several supporting stiffness in static components are calculated using ANSYS and measured by experiments, as listed in Table 2.

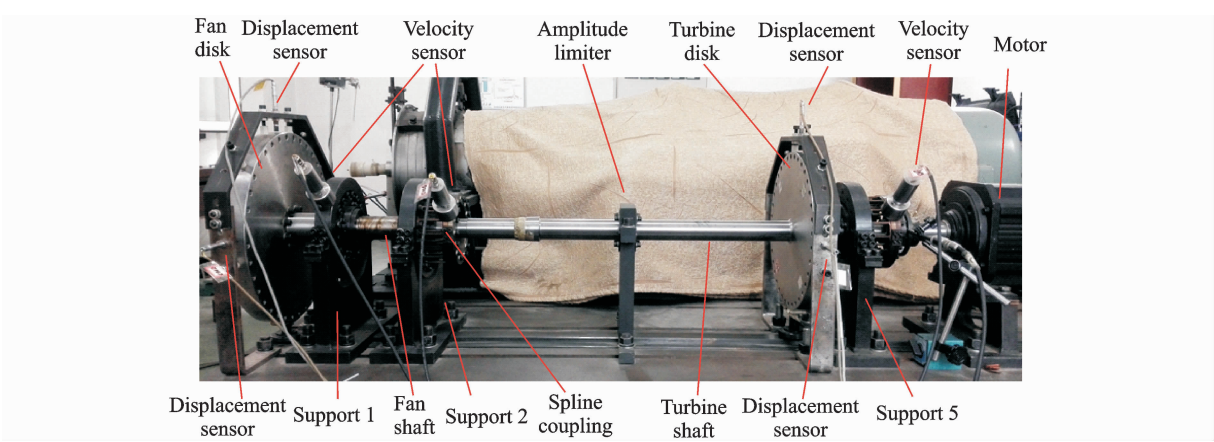

Fig. 9 Rotor test rig and sensors for measurement

Table 2 Supporting stiffness comparison

Stiffness	K_2/(N·m^{-1})	K_5/(N·m^{-1})
Calculated	$1.363\ 5\times10^6$	$1.366\ 6\times10^6$
Measured	$1.399\ 7\times10^6$	$1.403\ 2\times10^6$
Error/%	2.59	2.61

Dynamic balancing[10-11] of the experimental rotor system should be conducted prior to the actual operating process. The purpose of dynamic balancing is to readjust the mass distribution of

the rotor and to reduce the vibration level within permissible range[12-13].

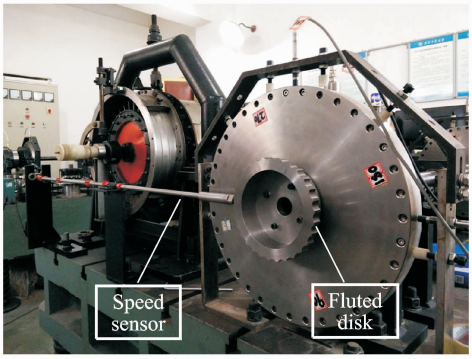

Fig. 10 Fluted disk and speed sensor

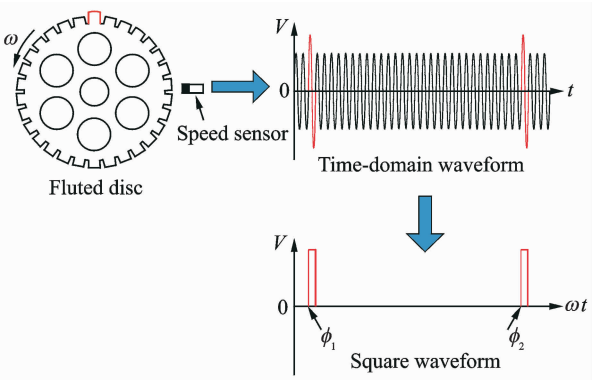

Fig. 11 Speed signal processing

In terms of the permissible ranges, it depends on specific situations and requirements. General speaking, the vibration amplitudes should not exceed designed maximum or limited values and the so-called effective dynamic balancing should reduce the vibration amplitudes at least more than 50% so that the rotor can pass critical speeds smoothly and safely[14], protecting the rotor from excessive and harmful vibrations.

To begin with the experiments, the initial bending of the rotor system[15] should be measured at low speed about 600 r/min. The least square influence coefficient method for computing balance corrections[16-17] is applied. The amplitude-frequency characteristic curves before and after balancing are shown in Fig. 12. After dynamic balancing, the vibration displacements of CH1—CH4 has been significantly reduced which meets the experimental requirement.

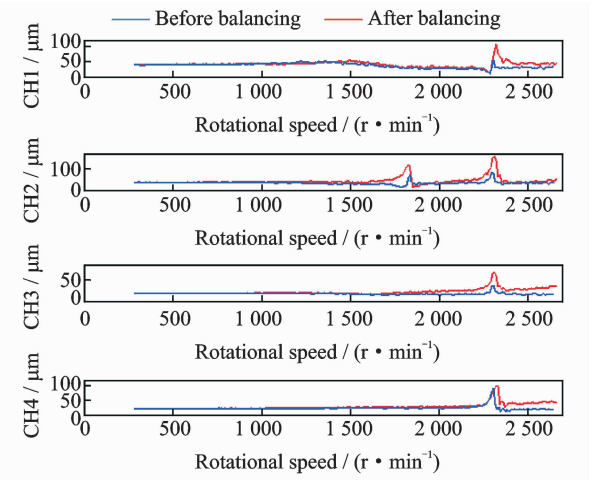

Fig. 12 Amplitude-frequency characteristic curves

3.2 Effects of tightening torque on dynamic characteristics

3.2.1 Critical speed analysis

To exert a certain amount of tightening torque, the utilization of torque wrenches is widespread[18]. In order to explore the influence of tightening torque on the critical speeds, the tightening torque is given three values including 60, 90 and 120 N • m.

As shown in Fig. 13, the first two critical speeds present an upward trend when tightening torque increases, and specifically the growth rates of the first-order and second-order critical speeds are 1.23% and 0.51%, respectively.

It can be seen that the tightening torque of the axial nut is more sensitive to the first critical speed than to the second one. Furthermore, changing the tightening torque can alter the connection stiffness of the shafts, thereby affecting the operating state of the entire rotor system. When increasing the tightening torque, the fan shaft and the turbine shaft tend to be an integral shaft.

The simulation results are compared with the experiment results which are obtained under the condition of maximum tightening torque (120 N• m) listed in Table 3. It can be seen that the relative errors of the first two critical speeds between simulation and experiment are rather small, which can prove that the simulation results are

believable and the simulation process is worth conducting in terms of the preliminary design.

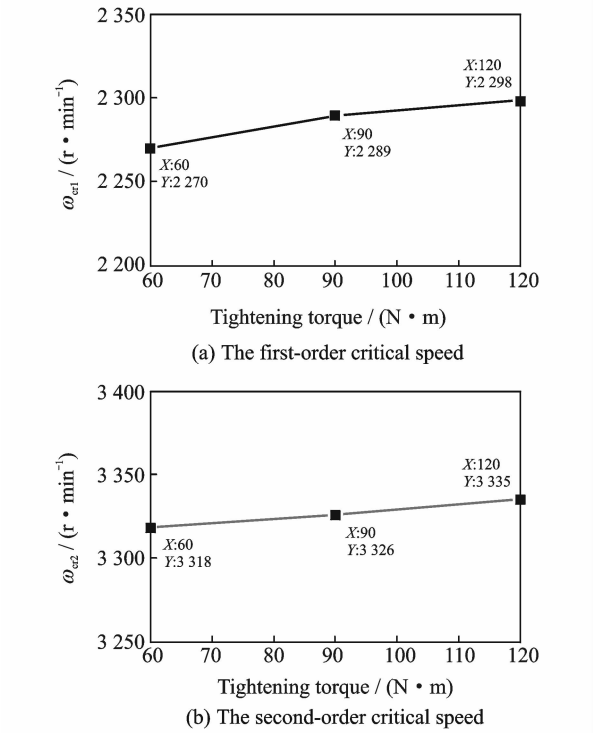

Fig. 13 Experimental critical speeds

Table 3 Critical speeds comparison

Critical speeds	First-order/ (r • min^{-1})	Second-order/ (r • min^{-1})
Simulation	2 298.515	3 345.339
Experiment	2 298	3 335
Error/%	1.26	1.58

3.2.2 Vibration mode analysis

In order to measure the first two vibration modes, four displacement sensors are distributed along the axial direction to measure displacements in the vertical direction simultaneously, as shown in Fig. 14, changing the tightening torque from 60 N • m to 120 N • m.

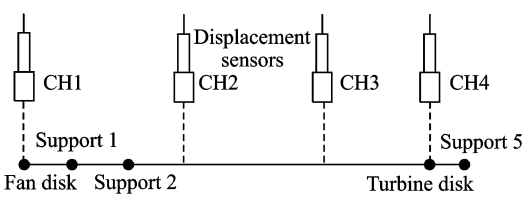

Fig. 14 Layout of displacement sensors for modal test

Considering that the pitching mode may occur, the vibration displacement of the fan disk (CH1) is used as the reference (The value is equal to −1), and then the other three measuring points (CH2—CH4) along the axial direction are normalized. According to the relative displacements of the four measuring points, the measured first two modes can be obtained by means of numerical fitting. The experimental first two modes are listed in Tables 4, 5, respectively.

Table 4 Experimental first-order mode

Tightening torque /(N • m)	CH1	CH2	CH3	CH4
60	−1	1.029 6	1.281 8	0.394 7
90	−1	1.047 1	1.288 6	0.413 6
120	−1	1.032 9	1.336 6	0.473 7

Table 5 Experimental second-order mode

Tightening torque /(N • m)	CH1	CH2	CH3	CH4
60	−1	−0.088 7	−0.534 2	−1.269 0
90	−1	−0.120 4	−0.565 4	−1.210 6
120	−1	−0.142 5	−0.626 3	−1.256 1

(1) The first mode

The effect of the tightening torque on the first mode is presented in Fig. 15. The arched vibration curves measured in the experiment are consistent with the ones calculated in the simulation, which suggests that a generally good agreement is obtained between the experimental and simulating results.

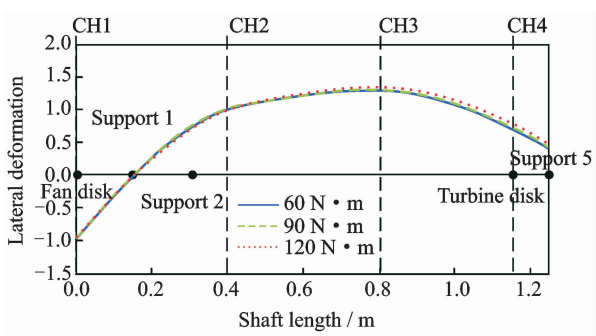

Fig. 15 Effect of tightening torque on the first-order mode

Through horizontal comparison in terms of different measuring positions, it can be seen clearly that a phase shift of 180° exists between the measuring position CH1 and the other three measuring positions. Through vertical comparison in terms of different tightening torques, the first vibration mode remain basically unchanged.

(2) The second mode

The effect of the tightening torque on the second mode is presented in Fig. 16. The arched vibration curves measured in the experiment are approximately consistent with the ones calculated in the simulation. Through horizontal comparison in terms of different measuring positions, it is shown that apparent phase shift does not exist among the measuring positions. Through vertical comparison of different tightening torques, the second vibration mode still remain essentially unchanged.

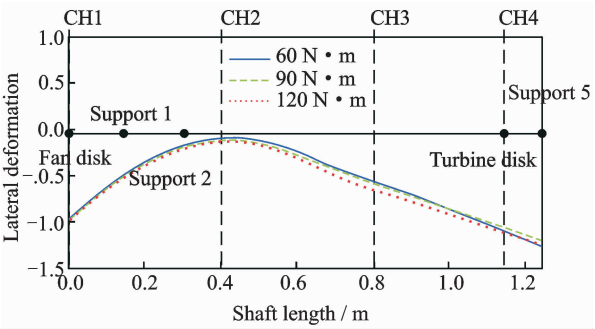

Fig. 16 Effect of tightening torque on the second-order mode

In summary, the experimental curves of vibration modes are in accordance with the simulated curves basically, and when increasing tightening torque, the first two vibration modes are essentially unchanged.

3.2.3 Unbalance response analysis

After the mass unbalance 0.3 g at 0 or at 90° is added on the fan disk or the turbine disk, the vibration amplitudes at the fan disk (CH1—horizontal, CH2—vertical) and at the turbine disk (CH3—horizontal, CH4—veritical) are measured to study the effect of tightening torque on the unbalance response.

(1) Unbalance response for first-order mode

The unbalance responses varying with tightening torques are shown in Fig. 17. The horizontal coordinate, i.e., the tightening torque, ranges from 60 N • m to 120 N • m, and the vertical coordinate, i.e., the displacement amplitude of unbalance response, varies from 60 μm to 90 μm.

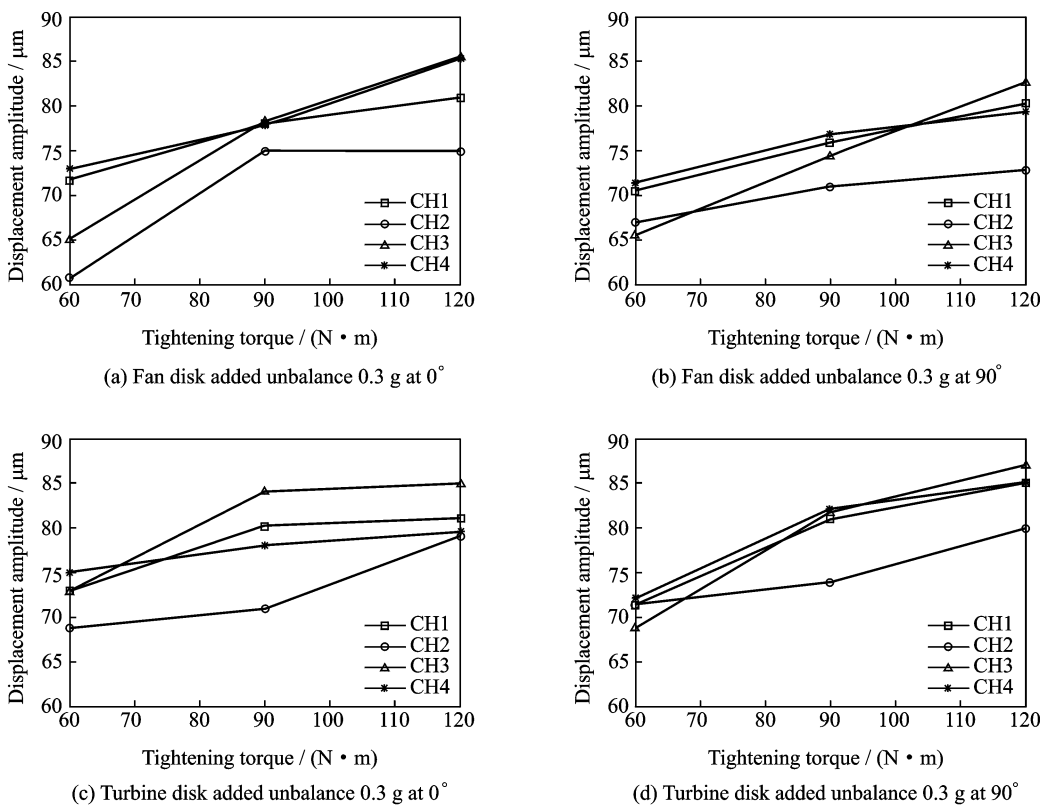

Fig. 17 Displacement amplitudes of unbalance response for first-order mode

(2) Unbalance response for second-order mode

The unbalance responses for second-order mode varying with tightening torque are shown in Fig. 18. The horizontal coordinate, i. e., the tightening torque, ranges from 60 N·m to 120 N·m. And the vertical coordinate, i. e., the displacement amplitude of unbalance response, in Figs. 18(a) and (b), varies from 10 μm to 120 μm, while in Figs. 18(c) and (d), it changes from 10 μm to 220 μm.

It is apparent that the range of value in the

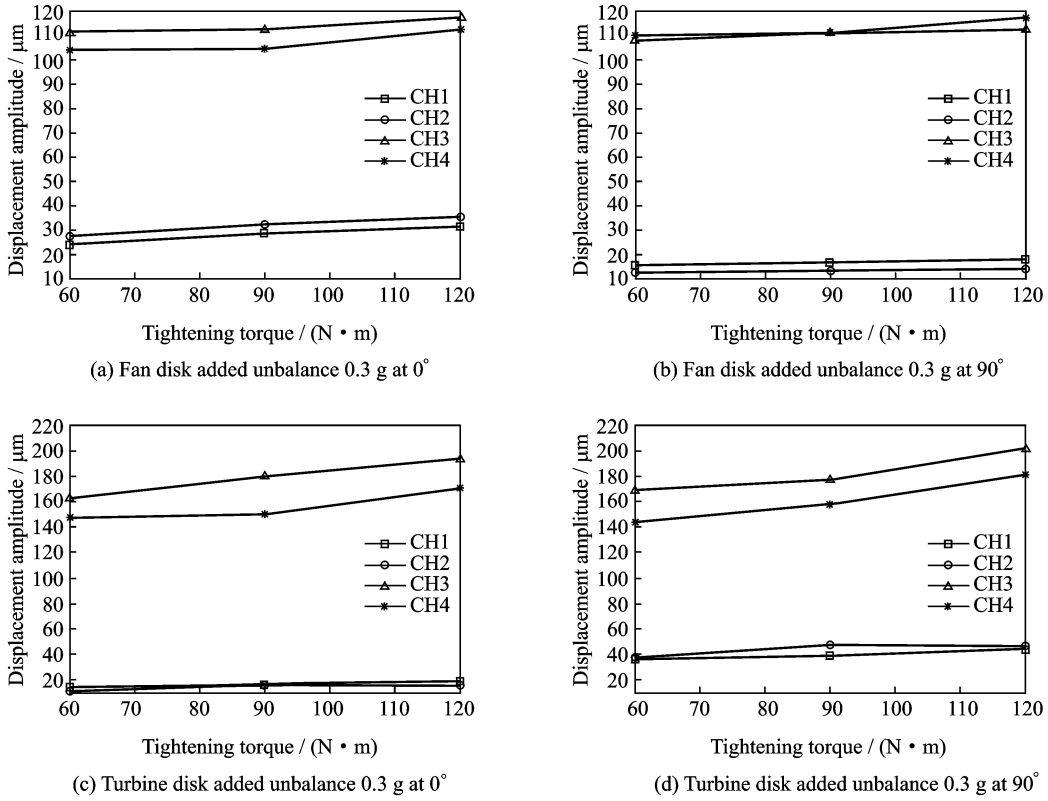

Fig. 18 Displacement amplitudes of unbalance response for second-order mode

unbalance response for second-order mode is much larger than the one for the first-order mode. The amplitudes of the unbalance response for second-order mode at the fan disk, is significantly less than the ones at the turbine disk, regardless of whether the mass unbalance is added on the fan disk or on the turbine disk, and of whether in the horizontal direction or in the vertical direction.

In summary, increasing the tightening torque can correspondingly increase the amplitudes of both unbalance responses with different degrees of variation. Different axial and circumferential positions of the mass unbalance result in various amplitudes of unbalance response and even the rates of change but the overall trend is that the amplitudes of unbalance response at all channels rise gradually with the increase of the tightening torque.

4 Conclusions

Through quantitatively analysis, the relative errors of the first two critical speeds between the simulation and the experimental results do not exceed 2%, which can verify that the simulation process is worth conducting in terms of the preliminary design.

Without changing the other experimental conditions and influence parameters, the growth rates of the first-order and second-order critical speeds are respectively 1.23% and 0.51% when the tightening torque varies from 60 N • m to 120 N • m. When increasing the tightening torque of the axial nut, the amplitudes of the unbalance response for both first-order and second-order modes gradually increase with varying de-

grees while the vibration modes remain unchanged on the whole. Changing axial and circumferential positions of the mass unbalance can result in various amplitudes of unbalance response and even the rates of change.

References:

[1] MARMOL R A, SMALLEY A J, TECZA J A, et al. Spline coupling induced nonsynchronous rotor vibration[J]. Journal of Mechanical Design, 1980, 102(1): 168-176.

[2] KU R C P, WALTON Jr J F, LUND J W. Dynamic coefficients of axial spline couplings in high-speed rotating machinery[J]. ASME Journal of Vibration and Acoustics, 1994, 116(2): 250-256.

[3] TJERNBERG A. Load distribution in the axial direction in a spline coupling[J]. Engineering Failure Analysis, 2001, 8(8): 557-570.

[4] AL-HUSSAIN K M. Dynamics stability of two rigid rotors connected by a flexible coupling with angular misalignment[J]. Journal of Sound and Vibration, 2003, 266(2): 217-234.

[5] LI Junhui, MA Yanghong, HONG Jie. Dynamic design method of spline joint structure for rotor system [J]. Aeroengine, 2009, 35(4): 36-39. (in Chinese)

[6] DENG Ming, LIU Changfu. Aero engine structural analysis[M]. Xi′an: Northwestern Polytechnical University Press, 2006. (in Chinese)

[7] BAKER W E, WESTINE P S, DODGE F T. Similarity methods in engineering dynamics: Theory and practice of scale modeling[M]. California: Spartan Books, 1973.

[8] MADENCI E, GUVEN I. The finite element method and applications in engineering using ANSYS[M]. New York: Springer, 2007.

[9] FU Caigao. Aero engine design manual (the 19th volume): Rotor dynamics and machine vibration[M]. Beijing: Aviation Industry Press, 2000. (in Chinese)

[10] DARLOW M S. Balancing of high-speed machinery [M]. New York: Springer-Verlag, 1989.

[11] VANCE J, ZEIDAN F, MURPHY B. Machinery vibration and rotor dynamics[M]. New Jersey: John Wiley & Sons, 2010.

[12] LIAO Mingfu. Rotor dynamics of aero engine[M]. Xi′an: Northwestern Polytechnical University Press, 2015. (in Chinese)

[13] CHEN Xi, LIAO Mingfu, LIU Zhanchi, et al. Modal balancing method for flexible rotors with elastic supports [J]. Journal of Nanjing University of Aeronautics & Astronautics, 2016, 48(3): 402-409. (in Chinese)

[14] XING Jian, HE Lidong, WANG Kai. Optimizing control for rotor vibration with magnetorheological fluid damper[J]. Transactions of Nanjing University of Aeronautics and Astronautics, 2014, 31(5): 538-545.

[15] WANG Siji, LIAO Mingfu. Study of techniques for rotor balance in situ[J]. Mechanical Science and Technology, 2005, 24(12): 1510-1514. (in Chinese)

[16] GOODMAN T P. A least-squares method for computing balance corrections[J]. ASME Journal of Manufacturing Science and Engineering, 1964, 86(3): 273-277.

[17] ZHANG Jingxuan, TANG Yunbing, LUO Guihuo. Improved least square influence coefficient methods[J]. Journal of Nanjing University of Aeronautics and Astronautics, 2005, 37(1): 110-113. (in Chinese)

[18] XU Shanhong. Mechanism analysis and experimental research for the sub-synchronous instability of turbopump[D]. Xi′an: Northwestern Polytechnical University, 2013. (in Chinese)

Ms. **Chen Xi** received her B. S. degree in Power Engineering of Aircraft from Northwestern Polytechnical University, Xi′an, China, in 2012. From September 2012 to present, she has worked as a candidate in Science and Technology of Aeronautics and Astronautics from Northwestern Polytechnical University, Xi′an, China. From February 2016 to January 2017, she had a one-year practice internship at Siemens Dynamowerk, Berlin, Germany. Her research has focused on rotor dynamics, field balancing and vibration measurement in the fields of aero-engines and wind turbines.

Prof. **Liao Mingfu** received his B. S. degree in Aero-engine Engineering from Northwestern Polytechnical University, Xi′an, China, in 1982 and the joint Ph. D. degree from Northwestern Polytechnical University, Xi′an, China and Technische Universität Berlin, Berlin, Germany, in 1995, respectively. From 1996 to present, he has worked as a full professor and doctoral supervisor in School of Power and Energy, Northwestern Polytechnical University. His research has focused on rotor dynamics, condition monitoring and fault diagnosis for aero-engines and gas turbines, and wind power technology. He is the vice chairman of the Rotor Dynamics Professional Committee in Chinese Society for Vibration Engineering.

Dr. **Li Quankun** received his B. S. degree in Power Engineering of Aircraft from Nanjing University of Aeronautics and Astronautics, Nanjing, China, in 2011 and his M. S. degree in Propulsion Theory and Engineering of Aeronautics and Astronautics from Northwestern Polytechnical University, Xi′an, China, in 2014, respectively. From January 2016, he has worked toward his Ph. D. degree at the Hong Kong Polytechnic University, Hong Kong, China. His research has focused on nonlinear dynamics analysis and fault diagnosis.

(Executive Editor: Xu Chengting)